Hindawi
Journal of Sensors
Volume 2021, Article ID 8816063, 18 pages
https://doi.org/10.1155/2021/8816063

Review Article

Accurate Calibration of a Self-Developed Vehicle-Borne LiDAR Scanning System

Ming Guo,[1,2,3,4] **Bingnan Yan**,[1] **Tengfei Zhou**,[1] **Deng Pan**,[5] **and Guoli Wang**[1,2,3,4]

[1]*School of Geomatics and Urban Spatial Informatics, Beijing University of Civil Engineering and Architecture, Beijing 102616, China*
[2]*Engineering Research Centre of Representative Building and Architectural Heritage Database, Ministry of Education, Beijing 100044, China*
[3]*Key Laboratory of Modern Urban Surveying and Mapping, National Administration of Surveying, Mapping and Geoinformation, Beijing 100044, China*
[4]*Beijing Key Laboratory for Architectural Heritage Fine Reconstruction & Health Monitoring, Beijing 102616, China*
[5]*School of Civil and Transportation Engineering, Beijing University of Civil Engineering and Architecture, Beijing 102616, China*

Correspondence should be addressed to Guoli Wang; wangguoli@bucea.edu.cn

Received 26 June 2020; Revised 1 January 2021; Accepted 22 January 2021; Published 9 February 2021

Academic Editor: Romeo Bernini

To obtain high-precision measurement data using vehicle-borne light detection and ranging (LiDAR) scanning (VLS) systems, calibration is necessary before a data acquisition mission. Thus, a novel calibration method based on a homemade target ball is proposed to estimate the system mounting parameters, which refer to the rotational and translational offsets between the LiDAR sensor and inertial measurement unit (IMU) orientation and position. Firstly, the spherical point cloud is fitted into a sphere to extract the coordinates of the centre, and each scan line on the sphere is fitted into a section of the sphere to calculate the distance ratio from the centre to the nearest two sections, and the attitude and trajectory parameters of the centre are calculated by linear interpolation. Then, the real coordinates of the centre of the sphere are calculated by measuring the coordinates of the reflector directly above the target ball with the total station. Finally, three rotation parameters and three translation parameters are calculated by two least-squares adjustments. Comparisons of the point cloud before and after calibration and the calibrated point clouds with the point cloud obtained by the terrestrial laser scanner show that the accuracy significantly improved after calibration. The experiment indicates that the calibration method based on the homemade target ball can effectively improve the accuracy of the point cloud, which can promote VLS development and applications.

1. Introduction

With the rapid development of information technology, geographic information data and geospatial data are increasingly playing important roles in urban construction and social services, which require faster updating and higher accuracy of data. Considerable research efforts have been devoted to the mobile mapping system (MMS), which can obtain spatial information quickly and efficiently to meet the needs of various applications [1, 2]. As a type of MMS, the VLS system integrates global navigation satellite systems (GNSS), inertial measurement units, LiDAR scanning systems, image acquisition systems, and time synchronization systems on a common vehicle platform [3]. During vehicle driving, it measures the information of roads and buildings on both sides in real time and obtains image data and point cloud data of the measured objects by the camera and LiDAR scanner. LiDAR technology has been widely used in environmental perception because it has the following advantages: it is fast, it can be highly automated, and it is not affected by illumination conditions [4]. Compared with other scanning methods, VLS has the advantages of high efficiency and strong flexibility and has been widely utilized to generate high-quality 3D geospatial information for urban environments [5]. In some practical applications, high-precision data are often needed, such as large-scale digital line drawing measurements. If

(a) (b)

Figure 1: The integrated spatial geometric position relationship between the LiDAR sensor and the IMU of the VLS system. (a) The self-developed VLS system is shown. (b) The geometric position and coordinate system of the LiDAR scanner and the IMU are shown, in which red represents the X-axis, blue represents the Y-axis, and green represents the Z-axis.

VLS data fail to meet the accuracy requirements for practical applications, then resource waste may occur. To take full advantage of the VLS system, the key is to improve the data accuracy of the VLS system. For this purpose, it is urgent to calibrate VLS systems to improve the data accuracy, so as to provide data support for intelligent maps, urban planning, smart cities, autonomous driving, and other applications.

As the main collection method of road and urban building geospatial information, the integration, calibration, and application of VLS systems have been current research hotspots for several years [6]. The full positioning potential of a VLS is determined not only by the accuracy of the individual sensors but also by the ability to accurately calibrate the entire system [7]. In addition, it will also be affected by multiple environmental factors, such as GNSS occlusion, detours, driving speed, and laser incident angle. Evidence for the above environmental factors was presented by Ma et al. [8] and Zhang et al. [9], although the impact of the environment is relatively weak. Besides, the internal calibration of the sensor is usually completed by the manufacturer at the factory, so it is not studied here. In order to obtain high-precision point cloud data, this paper focuses on the calibration of the external mounting parameters of the integrated system, that is, to estimate the translational (lever-arm) and rotational (boresight angles) offsets between the LiDAR sensor and the IMU position and orientation system [10, 11], as shown in Figure 1. Over the past few years, a great deal of research has been conducted in the area of mobile LiDAR system calibration, each of which has advantages and drawbacks. Song et al. proposed a method for detecting the single-sensor accuracy based on the calibration field to correct the accuracy of each sensor and system [12], which may ignore the effect of mutual interference between integrated sensors on system accuracy. Glennie proposed a method of rigorous calibration of the MMS system without the use of targets or external measurements. A planar feature based on the least-squares adjustment approach was utilized to derive an optimal solution for the laser's internal calibration parameters and boresight offsets [13]. However, experiments require a large number of planes in the experimental scene. On the basis of feature points, a rigorous registration approach for a time-variant helmet transformation model was proposed by Han et al. By making use of this model and a few calibration points, most positioning errors due to the loss of satellite signals can be eliminated significantly [14]. However, manual identification of LiDAR points corresponding to known calibration points may become tedious when processing large amounts of data. He et al. used pairwise multitype 3D geometric features (i.e., points, lines, and planes) to derive the extrinsic parameters between 2D LiDAR and GNSS/IMU [15]. However, when the initial parameters are considerably inaccurate, the segments and derived weights may not be reliable. Tian et al. performed a method based on the feature plane to estimate the installation angles between the laser scanner and the inertial navigation system (INS) using the vertical facade of a building wall [16]. This method requires planes that can be easily extracted in the experimental scene, and a large amount of occlusion is likely to affect the experimental results. Hong et al. proposed an MMS method that is calibrated with a terrestrial laser scanner (TLS), and it extracts point and plane features from TLS data and matches them with the features extracted from the mobile laser scanning data and the captured images [17]. The essence of this method is the calibration of feature points and feature planes. Julge et al. proposed a calibration method based on bound optimization by quadratic approximation to identify the boresight angles of the mobile laser scanning system [18]. Chan et al. presented a system calibration method based on multiple features, and it used a plane feature model and a rigorous three-dimensional catenary curve model to augment the calibration [19]. However, these two methods are relatively complex. Zhang et al. used point clouds collected by unmanned aerial vehicles as corrective control points for vehicle point clouds [20]. However, this method cannot be widely used due to the limitations of the flight area. Li et al. proposed an automatic boresight self-calibration strategy for MMSs using an acquired multistrip point cloud by an ICP (Iterative Closest Point) algorithm. They calibrated the system under the assumption that the lever-arm was accurately measured without calibration [21]. Nevertheless, the ICP would fail in cases where the initial estimates of boresight angles cause significant misalignments. Ravi et al. proposed a fully automated targetless calibration technique to

estimate the mounting parameters related to the onboard LiDAR units and the GNSS/IMU unit for an MMS with spinning multibeam laser units [7]. This method is also affected by the initial accuracy. Although many calibration methods have been proposed, most of them have certain limitations. While point-based calibration techniques using a checkerboard or ground control points can represent practical solutions for system calibration, it is difficult to extract accurate corner or edge points from sparse point clouds generated by the VLS system due to its low resolution. Moreover, tracing accurate object boundaries in a LiDAR point cloud dataset is very difficult [22]. Therefore, a special target ball that can accurately obtain the coordinates of feature points is developed in this paper. A horizontal bubble and a reflective sheet are installed on the top of the target ball [23], and they are used as centering devices to ensure that the coordinates of the centre of the sphere are obtained from the VLS system and the total station measurement is in the same position. Based on the calibration of the feature point, this paper proposes a calibration strategy using the target ball to estimate the system mounting parameters. In the vehicle scanning point cloud data, the target ball is obtained by fitting multiple points on the spherical surface and the fitting accuracy is at the millimetre level. According to the parameters of the scan line closest to the centre of the sphere, the parameters of the centre of the sphere are calculated by linear interpolation. Based on the calibration model, the parameters of translational and rotational offsets are calculated by the least-squares adjustment iteration and then the mounting parameters of the system are estimated.

The unique point of this paper is to propose a novel method to obtain the spherical centre parameters for calibration, which is less affected by the boundary of point cloud and noise points, and also less affected by the initial estimation of boresight angles and the experimental site. This method is more accurate and simpler than previous studies and effectively compensates for the limitation of inaccurate feature point extraction. In Section 2, we introduce the calibration method in detail. Then, we use the method to calibrate the self-developed VLS system; the experiment is shown in Section 3. In Section 4, we discuss the point cloud accuracy after calibration. The last section obtains the conclusion with plans for future studies.

2. Calibration Method

The three-dimensional point coordinates of the VLS system are obtained by the registration of the point coordinates collected by LiDAR scanner with the position and attitude information collected by the inertial navigation system. In fact, this is a process of spatial coordinate conversion, which usually needs three common control points to complete. Since the various hardware sensors of the VLS system are integrated on the vehicle platform with a relatively fixed geometric relationship, according to the hardware integration mode, a space coordinate transformation model can be derived for calibration, and use the least-squares adjustment method to solve the translation and rotation parameters of the LiDAR sensor relative to IMU.

2.1. Calibration Model. The calibration model is based on the principle of system hardware integration and positioning. It is a three-dimensional coordinate conversion model, as shown in equation (1). In the process of the LiDAR and IMU coordinate system conversion, a rotation error vector $\Delta R_0 = [\Delta\alpha, \Delta\beta, \Delta\gamma]^T$ and a translation error vector $\Delta T_0 = [\Delta X_0, \Delta Y_0, \Delta Z_0]^T$ are introduced. The rotation angle error rotating around the X, Y, and Z axes are $\Delta\alpha$, $\Delta\beta$, and $\Delta\gamma$, respectively, and the translation values are ΔX_0, ΔY_0, and ΔZ_0, respectively.

$$\begin{bmatrix} X_{\mathrm{ECEF}} \\ Y_{\mathrm{ECEF}} \\ Z_{\mathrm{ECEF}} \end{bmatrix} = R_M \left[R_N \left[\Delta R_0 R_0 \begin{bmatrix} X_L \\ Y_L \\ Z_L \end{bmatrix} + \begin{bmatrix} X_{\mathrm{LI}} \\ Y_{\mathrm{LI}} \\ Z_{\mathrm{LI}} \end{bmatrix} + \begin{bmatrix} \Delta X_0 \\ \Delta Y_0 \\ \Delta Z_0 \end{bmatrix} \right] \right] + \begin{bmatrix} X_{\mathrm{GPS}} \\ Y_{\mathrm{GPS}} \\ Z_{\mathrm{GPS}} \end{bmatrix}, \tag{1}$$

where R_0 and $[X_{\mathrm{LI}}, Y_{\mathrm{LI}}, Z_{\mathrm{LI}}]^T$ are the spatial rotation matrix and translation matrix from the scanner coordinate system to the IMU coordinate system, respectively, which are composed of initial values of the system mounting parameters, and $[X_L, Y_L, Z_L]^T$ is the coordinate of a point in the scanner coordinate system. R_N is the rotation matrix from the IMU coordinate system to the local horizontal coordinate system, which is composed of the roll, pitch, and heading measured by the IMU. Since the origin of these two coordinate systems is the same, only the rotation matrix is needed to complete the conversion. In addition, R_M and $[X_{\mathrm{GPS}}, Y_{\mathrm{GPS}}, Z_{\mathrm{GPS}}]^T$ are the rotation matrix and translation matrix from the local horizontal coordinate system to the ECEF (earth-centred, earth-fixed) coordinate system, respectively; R_M is composed of the geodetic latitude and geodetic longitude, and $[X_{\mathrm{ECEF}}, Y_{\mathrm{ECEF}}, Z_{\mathrm{ECEF}}]^T$ is the coordinate of the point in the ECEF coordinate system.

According to the model, all the parameters except the error vector are known, which can be calculated by the least-squares indirect adjustment method. Taking the data $[X_q, Y_q, Z_q]^T$ measured by the total station as the ECEF coordinate value, the following error equation is derived after linearization of equation (1), where $V = [v_x, v_y, v_z]^T$ represents the correction value vector of coordinates:

$$v_x = X_L - X_q + \frac{\partial X_L}{\partial \alpha}\Delta\alpha + \frac{\partial X_L}{\partial \beta}\Delta\beta + \frac{\partial X_L}{\partial \gamma}\Delta\gamma + \frac{\partial X_L}{\partial \Delta X_0}\Delta X_0 + \frac{\partial X_L}{\partial \Delta Y_0}\Delta Y_0 + \frac{\partial X_L}{\partial \Delta Z_0}\Delta Z_0,$$

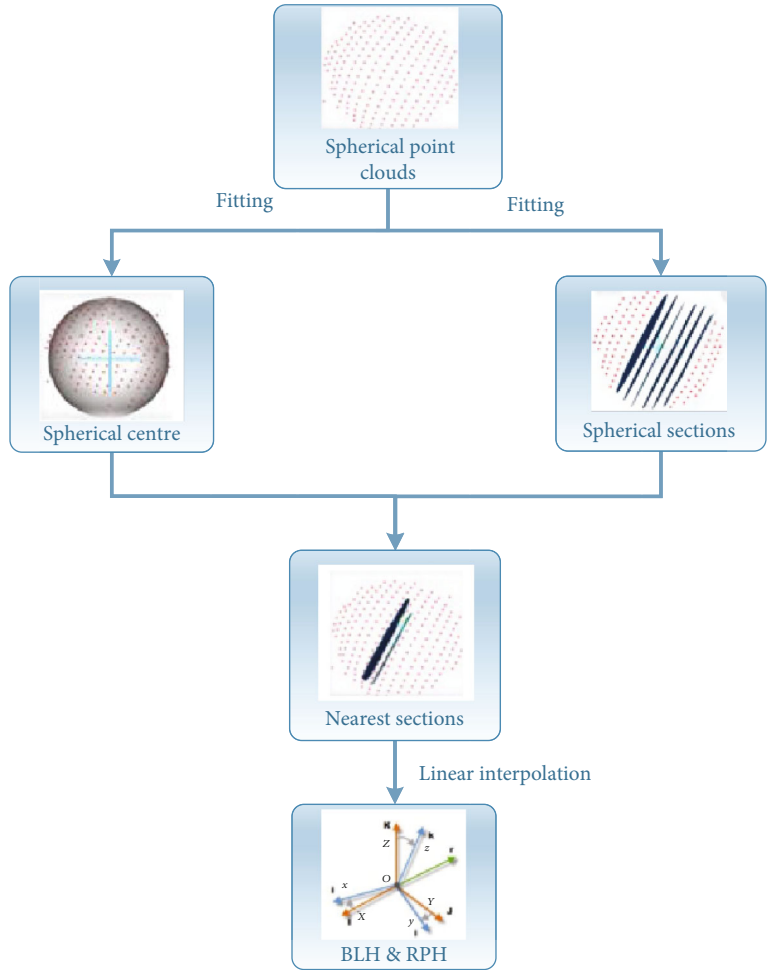

Figure 2: Flowchart for calculating parameters of the target centre. The figure shows the process of fitting the sphere from the point cloud and solving the parameters of the centre: B, L, and H represent geodetic latitude, geodetic longitude, and geodetic height, respectively; R, P, and H represent the attitude angle roll, pitch, and heading, respectively.

$$\begin{aligned} v_y &= Y_L - Y_q + \frac{\partial Y_L}{\partial \alpha}\Delta\alpha + \frac{\partial Y_L}{\partial \beta}\Delta\beta + \frac{\partial Y_L}{\partial \gamma}\Delta\gamma + \frac{\partial Y_L}{\partial \Delta X_0}\Delta X_0 \\ &\quad + \frac{\partial Y_L}{\partial \Delta Y_0}\Delta Y_0 + \frac{\partial Y_L}{\partial \Delta Z_0}\Delta Z_0, \\ v_z &= Z_L - Z_q + \frac{\partial Z_L}{\partial \alpha}\Delta\alpha + \frac{\partial Z_L}{\partial \beta}\Delta\beta + \frac{\partial Z_L}{\partial \gamma}\Delta\gamma + \frac{\partial Z_L}{\partial \Delta X_0}\Delta X_0 \\ &\quad + \frac{\partial Z_L}{\partial \Delta Y_0}\Delta Y_0 + \frac{\partial Z_L}{\partial \Delta Z_0}\Delta Z_0. \end{aligned} \tag{2}$$

Here, equation (2) is transformed into matrix form as a least-squares indirect adjustment error equation shown in equation (3), where B is the coefficient matrix, X is the error parameter, and L is the constant term.

$$\begin{aligned} V &= BX - L, \\ X &= [\Delta\alpha, \Delta\beta, \Delta\gamma, \Delta X_0, \Delta_0, \Delta Z_0]^T, \\ L &= \left[X_L - X_q, Y_L - Y_q, Z_L - Z_q\right]^T, \end{aligned}$$

$$B = \begin{bmatrix} \frac{\partial X_L}{\partial \alpha} & \frac{\partial X_L}{\partial \beta} & \frac{\partial X_L}{\partial \gamma} & \frac{\partial X_L}{\partial \Delta X_0} & \frac{\partial X_L}{\partial \Delta Y_0} & \frac{\partial X_L}{\partial \Delta Z_0}\frac{\partial X_L}{\partial \Delta Z_0} \\ \frac{\partial Y_L}{\partial \alpha} & \frac{\partial Y_L}{\partial \beta} & \frac{\partial Y_L}{\partial \gamma} & \frac{\partial Y_L}{\partial \Delta X_0} & \frac{\partial Y_L}{\partial \Delta Y_0} & \frac{\partial Y_L}{\partial \Delta Z_0} \\ \frac{\partial Z_L}{\partial \alpha} & \frac{\partial Z_L}{\partial \beta} & \frac{\partial Z_L}{\partial \gamma} & \frac{\partial Z_L}{\partial \Delta X_0} & \frac{\partial Z_L}{\partial \Delta Y_0} & \frac{\partial Z_L}{\partial \Delta Z_0} \end{bmatrix}. \tag{3}$$

According to the principle of the least-squares method, the error equation must satisfy

$$V^T PV = \min. \tag{4}$$

The normal equation is derived as equation (5), where P is the weight matrix and the weight of the equal precision observation is 1.

$$B^T PBX = B^T PL. \tag{5}$$

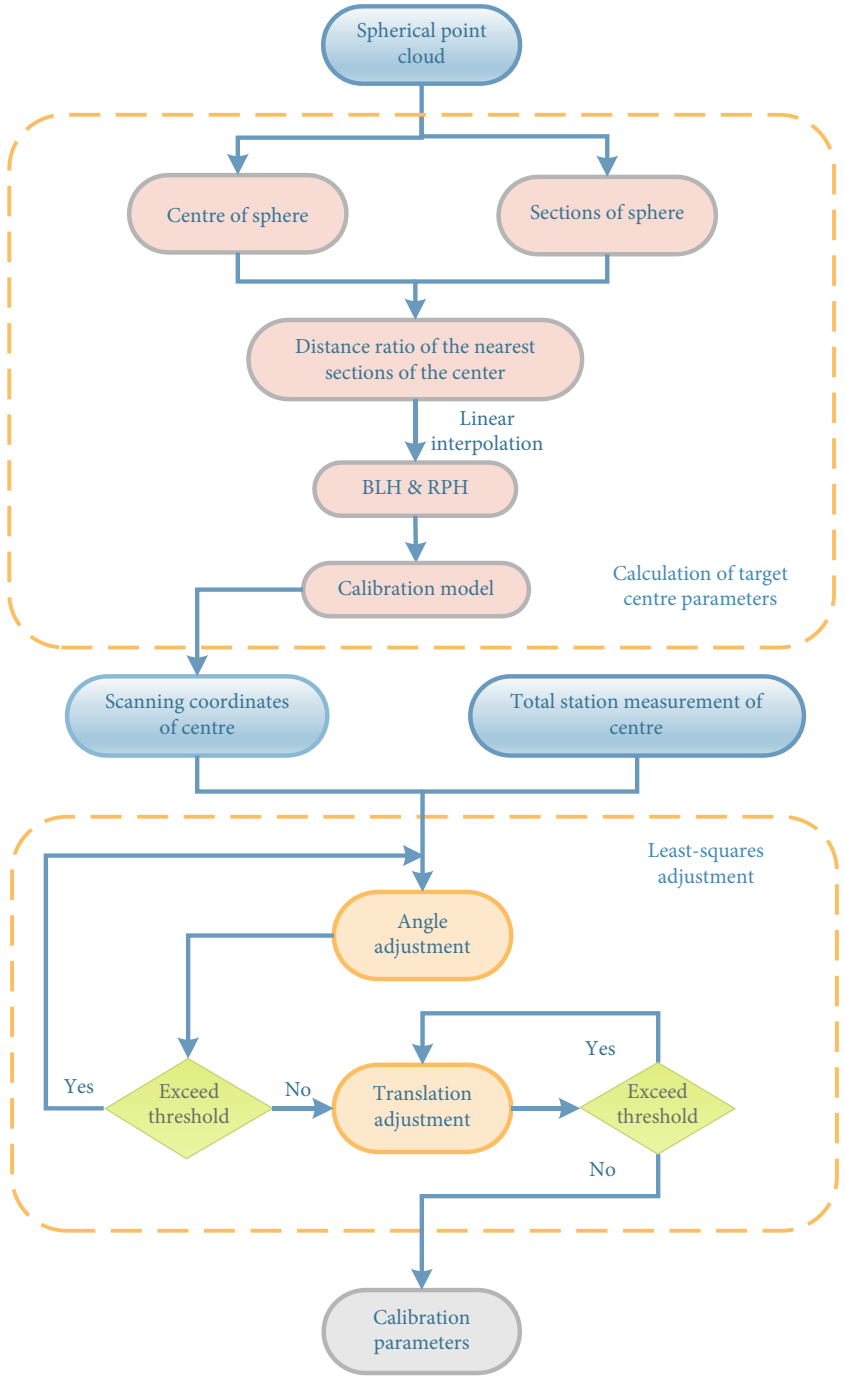

Figure 3: Flowchart for the calibration process. According to the calibration model, the relevant parameters of the spherical target centre are first calculated and then the true value of the spherical target centre is calculated from the total station measurement data. After two least-squares adjustments, the rotation and translation parameters of the system are estimated.

So, we have

$$X = \left(B^T PB\right)^{-1} B^T PL. \tag{6}$$

The iterative calculation is enforced until the error correction value is less than a certain threshold value; it is considered that the calculated values of $\Delta\alpha$, $\Delta\beta$, $\Delta\gamma$, ΔX_0, ΔY_0, and ΔZ_0 are optimal.

2.2. Calculation of Target Centre Parameters. The calibration strategy takes the centre of the spherical target as the calibration control point, and it is necessary to determine the coordinates, attitude values, trajectory values, and other related parameters of the centre in the calibration. However, the parameters of the target centre cannot be scanned directly, only the data of the spherical target surface can be collected in the scanning process of the VLS system. Therefore, these

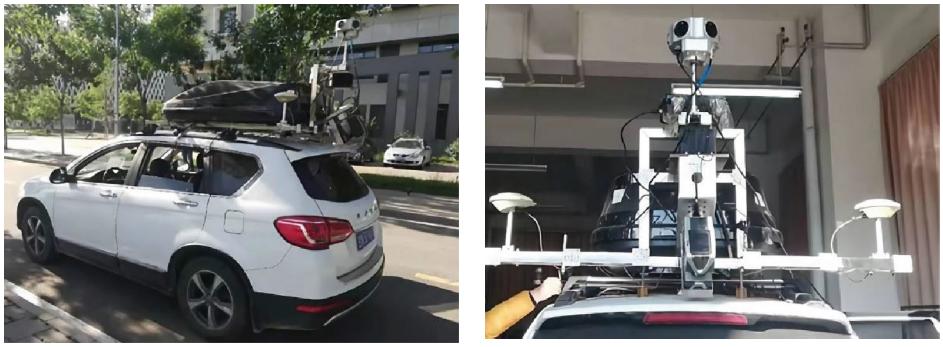

(a) (b)

Figure 4: Self-developed vehicle-borne LiDAR scanning system (integrated GNSS, scanner, IMU, panoramic camera, and time synchronizer). (a) In operation. (b) Installation.

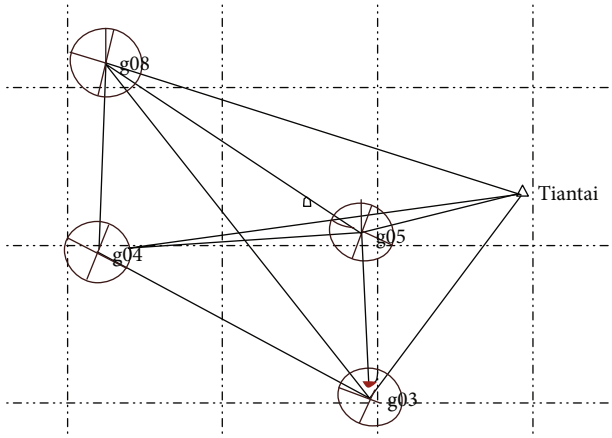

(a)

Adjustment ECEF coordinate

ID	X error (m)	Y error (m)	Z error (m)	3D error (m)
g03	0.002	0.003	0.003	0.005
g04	0.002	0.003	0.003	0.005
g05	0.002	0.003	0.003	0.004
g08	0.002	0.003	0.003	0.005
Tiantai	?	?	?	?

Adjustment geodetic coordinate

ID	Latitude	Longitude	Height (m)	Height error (m)
g03	N**** 06921•	E****** 3980•	* .041	0.004
g04	N**** 04016•	E****** 5218•	* .257	0.004
g05	N**** 44959•	E****** 0448•	* .451	0.004
g08	N**** 93515•	E****** 7350•	* .562	0.004

(b)

Figure 5: Solving the coordinates of control points. (a) GNSS network constructed by control points, in which triangles represent known long-term static positioning points and others were unknown points. (b) The error of control points in different coordinate systems.

centre parameters need to be calculated before calibration, using the linear interpolation method based on the known points on the surface of the target ball (see Figure 2). Firstly, the spherical points are found in the whole scene point cloud and fitted to a sphere, and then the centre coordinates of the sphere are calculated. Then, the spherical points on the same scanning line, that is, the points with the same ID, are fitted into a cross-section of the sphere, and the distance ratio of

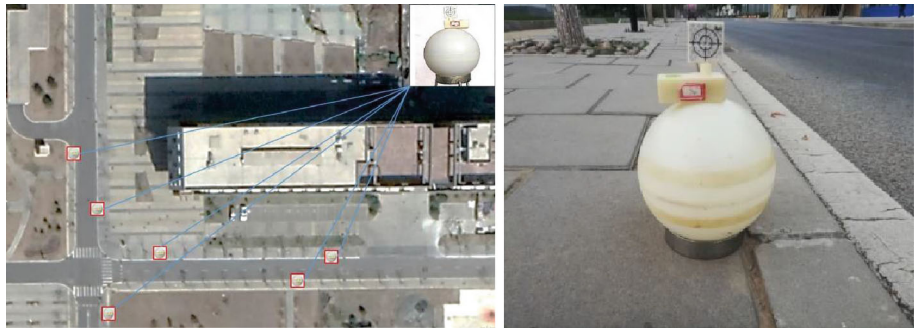

(a)

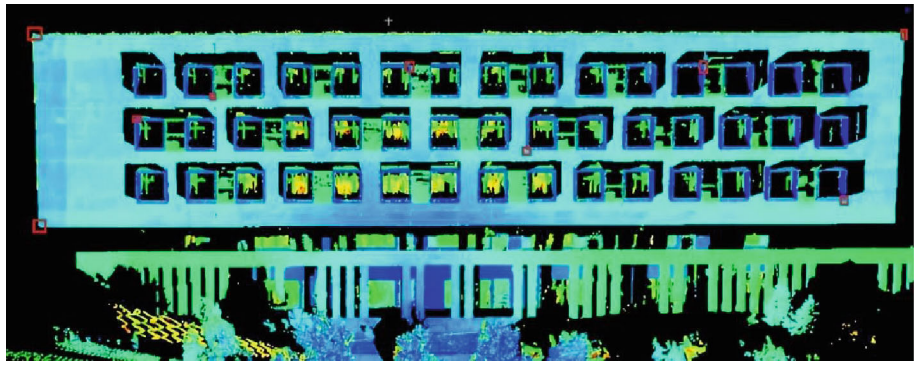

(b)

Figure 6: Distribution of target balls and some feature points. (a) The red box shows the position of the control points of the target ball, the upper right corner is the target ball, and the right side is a target ball placed in the experiment. (b) The red box shows the position of some other feature points.

the two sections nearest to the centre of the sphere is calculated. Finally, according to the scanning line parameters and the distance ratio of the two sections, the trajectory and attitude parameters corresponding to the centre of the sphere are calculated by the linear interpolation algorithm.

2.3. Calibration Process. Generally, calibration requires more than three common coordinate points of known parameters, which can be carried out according to the following process, as shown in Figure 3:

(i) Calculate the parameters and coordinates of the spherical target centre according to the point cloud

(ii) Calculate the coordinates of the spherical target centre measured by a total station: the total station directly measures the coordinate of the reflector on the ball and then calculates the centre coordinate of the sphere according to the designed fixed value of the target ball from the reflector centre to the spherical centre. Because the measurement accuracy of the total station is millimetre level, which is higher than that of the VLS system, the measured value is taken as the true value of the centre of the target ball

(iii) Estimate the mounting parameters: according to the calibration model, the mounting parameters are solved by the least-squares adjustment, and the rotation angle threshold is set as 0.001°, and the translation threshold is set as 0.001 m. When the angle adjustment satisfies the iterative precision threshold, the results are input to the model, and then the translation parameters are solved. If the error is greater than the set threshold, the iteration calculation will be rigorously enforced until the threshold is met, and the mounting parameters of the system will be estimated

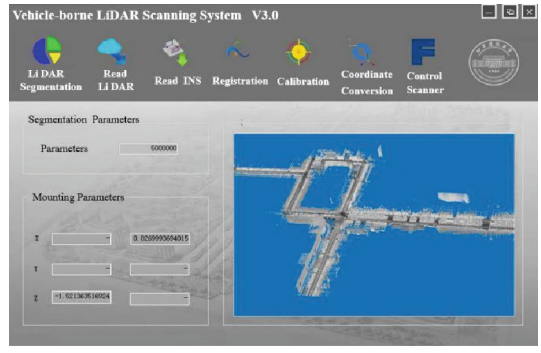

Figure 7: Software processing interface. The programming languages are C++ and C#, the platform is Visual Studio, the functional buttons are on top of the interface, the input system parameters are in the left text box, and the calculated point clouds are displayed on the right side.

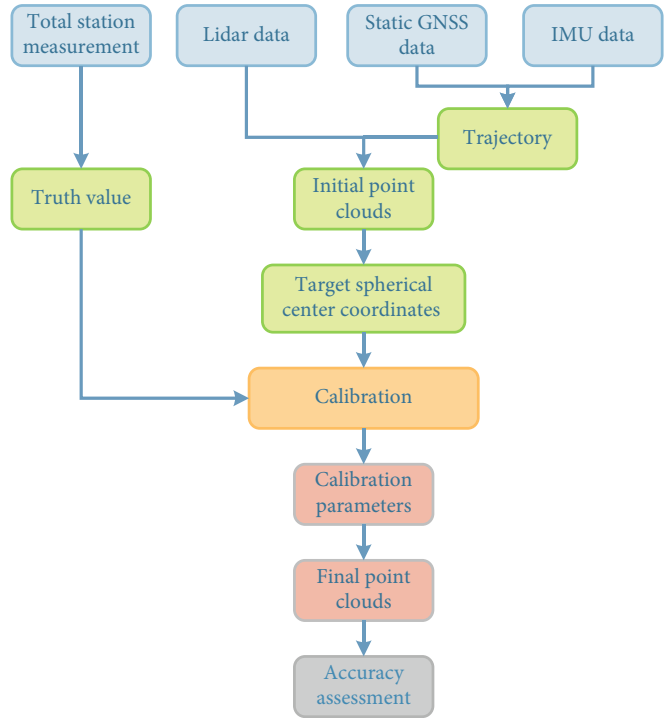

Figure 8: Data processing flowchart. The figure shows the process of data processing.

Table 1: Target centre coordinates and feature point coordinates.

	Total station measurement data			Precalibration data			Postcalibration data		
	X (m)	Y (m)	Z (m)	X (m)	Y (m)	Z (m)	X (m)	Y (m)	Z (m)
1	*** 182.4910	*** 441.3897	43.4003	*** 182.4513	*** 441.1347	43.6760	*** 182.5283	*** 441.4012	43.5283
2	*** 187.1674	*** 449.0007	43.2902	*** 187.1387	*** 448.8243	43.5336	*** 187.2397	*** 449.0243	43.3751
3	*** 134.9624	*** 485.2753	43.6783	*** 135.1172	*** 485.2248	43.8000	*** 134.9595	*** 485.1882	43.5949
4	*** 127.3952	*** 504.1670	43.7466	*** 127.6272	*** 504.1228	43.9040	*** 127.3965	*** 504.1080	43.7352
5	*** 150.8765	*** 450.9409	44.1269	*** 150.9997	*** 450.0861	44.2871	*** 150.9021	*** 450.9888	44.2185
6	*** 135.7534	*** 439.6988	43.8042	*** 135.5178	*** 439.5747	43.6700	*** 135.7389	*** 439.7168	43.7419
7	*** 126.1346	*** 456.8452	45.8364	*** 126.2363	*** 457.0387	45.6534	*** 126.1863	*** 456.9375	45.7618
8	*** 143.8149	*** 440.2873	44.6958	*** 143.8795	*** 440.4325	44.8494	*** 143.8238	*** 440.3018	44.7471
9	*** 165.3027	*** 498.1976	47.2546	*** 165.4311	*** 498.3696	47.3778	*** 165.3392	*** 498.2589	47.3170
10	*** 172.6233	*** 494.5018	53.4689	*** 172.7075	*** 494.6849	53.6345	*** 172.6507	*** 494.5580	53.5487

3. Calibration Experiment

3.1. Self-Developed VLS System. The experimental data of this paper is drawn from a self-developed VLS system, which integrates two GNSS receivers, an IMU, a three-dimensional laser scanner, a panoramic camera, and a time synchronizer (see Figure 4). In the system work, the GNSS/INS postprocessing process of the POS LV 220 sensor can attain a plane accuracy of 2 cm, an elevation accuracy of 5 cm, and a rolling/pitching and heading accuracy of 0.02° and 0.025°, respectively [24]. The scanner adopts the Faro Focus 3D 120, which is installed at the rear of the vehicle, and the data is collected using the line scanning mode with a resolution of 100 m/8 mm. The panoramic camera is used to obtain image information, and the time synchronizer realizes the time consistency of various sensor data. System positioning used the GNSS and IMU in conjunction to continuously provide accurate time, positional, and orientational solutions for a moving platform in real time, with very high accuracy [25, 26]. To minimize any potential sensor instability as much as possible, the VLS system is fixed on a metal frame on top of the vehicle.

3.2. Solve Coordinates of Control Points. A high-precision control network is an important prerequisite for the experiment, which guarantees the accuracy of the experimental data [27]. Before the experiment, static GNSS observations and International GPS Service (IGS) were used to remeasure

Table 2: Coordinate error of point cloud data and total station measurement data after calibration.

	ΔX (m)	ΔY (m)	ΔZ (m)	RMS error (m)
1	0.0373	0.0115	0.1280	0.0773
2	0.0723	0.0236	0.0849	0.0657
3	-0.0029	-0.0871	-0.0834	0.0696
4	0.0013	-0.0590	-0.0114	0.0346
5	0.0256	0.0479	0.0916	0.0614
6	-0.0145	0.0180	-0.0623	0.0383
7	0.0517	0.0923	-0.0746	0.0747
8	0.0089	0.0145	0.0513	0.0311
9	0.0365	0.0613	0.0624	0.0547
10	0.0274	0.0562	0.0798	0.0585
RMS error (m)	0.0351	0.0548	0.0784	0.0588
	0.046			

Table 3: Comparison of the relative accuracy between VLS system data and total station measurement data (error 1 and error 2 represent distance error before and after calibration, respectively).

	Total station measurement data (m)	Precalibration point cloud data (m)	Postcalibration point cloud data (m)	Error 1 (m)	Error 2 (m)
1	7.5457	7.5596	7.5370	0.0139	-0.0087
2	8.9349	9.0030	8.9630	0.0681	0.0281
3	64.6947	64.7478	64.7129	0.0531	0.0182
4	83.5307	83.4468	83.4980	-0.0839	-0.0327
5	63.5752	63.6020	63.5701	0.0268	-0.0051
6	81.3449	81.3072	81.3375	-0.0377	-0.0074
7	20.3522	20.2961	20.3405	-0.0561	-0.0117
8	74.785	74.8495	74.8066	0.0645	0.0216
9	2.3324	2.3910	2.3456	0.0586	0.0132
10	1.5648	1.6306	1.5814	0.0658	0.0166
RMS error (m)				0.0565	0.0184

the coordinates of the control points of the primary control network. Four ground control points were selected to set up the GNSS base station in the area with wide- and small-signal interference, and static observations were carried out simultaneously with the known control point of the rooftop. To ensure the accuracy of the data, we conducted three 24-hour observations and combined the static data, precise ephemeris, and IGS station data for the baseline solution and adjustment processing, and the accuracy of the control points was 5 mm (see Figure 5).

3.3. Experimental Data Acquisition. On the basis of the primary control network, a high-precision total station with an accuracy of $0.5''$ was used to encrypt the control network (see Figure 6). A large number of target balls were arranged within the observable range of the scanner, and they were evenly distributed on both sides of the road. The centre of the spherical target was taken as the calibration control point to calibrate the system parameters. Additionally, the window corner, billboard, and other features were also observed to verify the calibration accuracy. Each feature point was observed by four observations, and the average value was taken as the coordinate of the feature point for subsequent accuracy evaluation. To avoid the problem of point cloud caused by GNSS signal loss and vehicle vibration, the experimental site was chosen on a flat road with a wide visible area. The data were collected by the self-developed VLS system, and the vehicle was driven slowly and uniformly to ensure the quality of the observation data.

3.4. Experimental Data Processing. In the experiment, four kinds of data were collected: total station measurement data, GNSS static observation data, inertial navigation observation data, and point clouds. The collection and processing of point clouds were based on the self-programming software developed using the C++ and C# languages on the Visual Studio platform. Its main functions included the initial LiDAR data segmentation, LiDAR data and INS data reading, data registration, system calibration, coordinate conversion, and control scanner (see Figure 7). The data processing was mainly completed by data registration and system calibration modules of the point cloud solution software, which

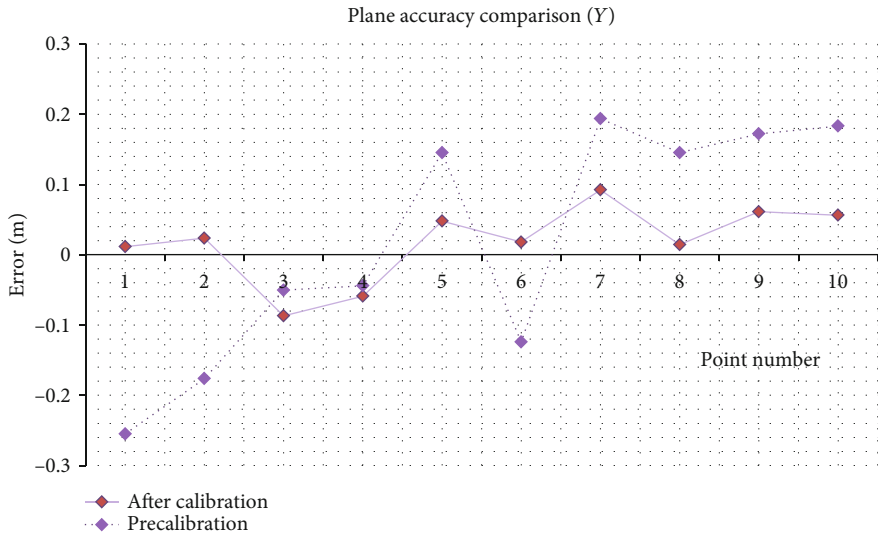

(a)

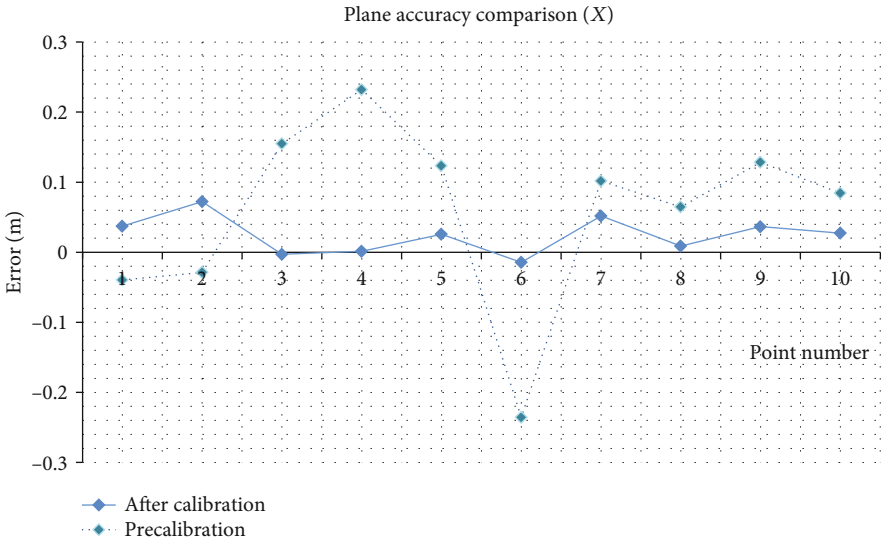

(b)

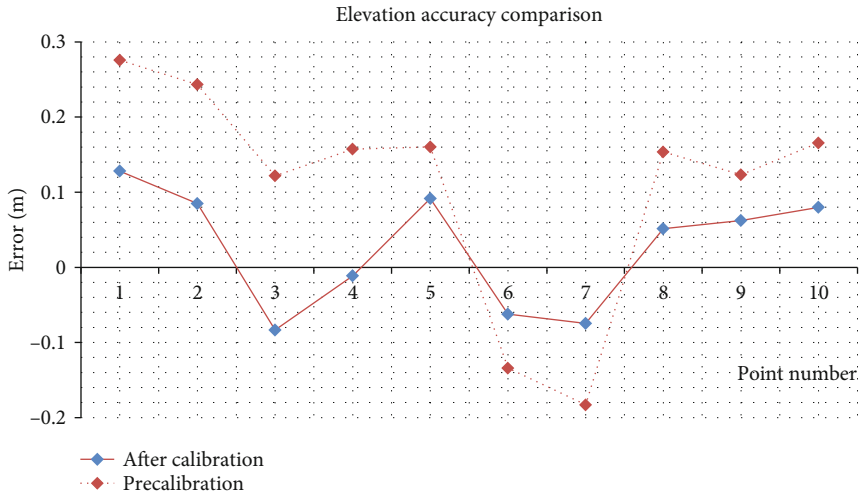

(c)

Figure 9: Continued.

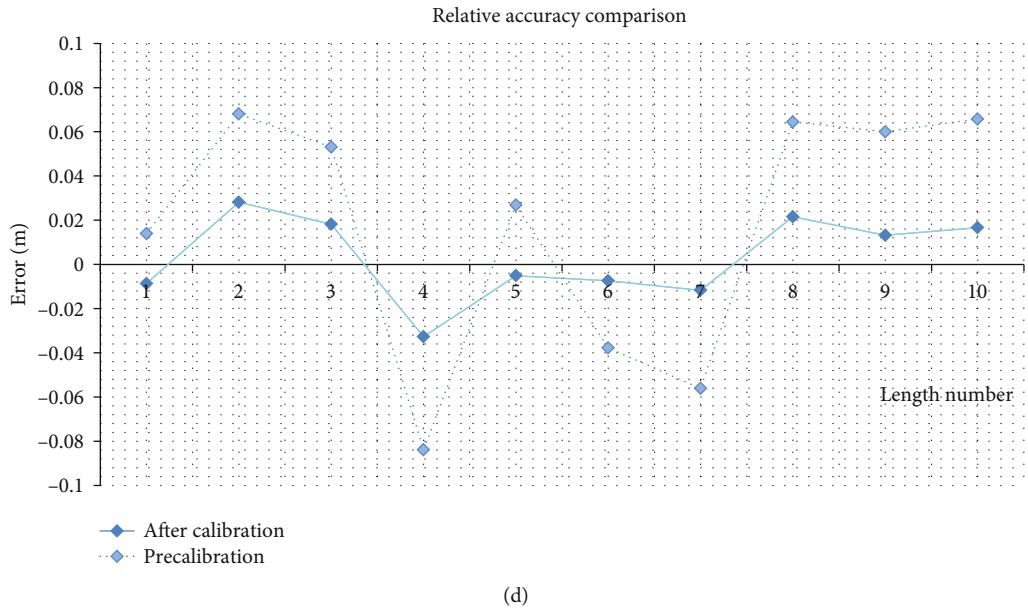

(d)

FIGURE 9: Accuracy comparison. (a) Y-direction accuracy comparison, (b) X-direction accuracy comparison, (c) elevation accuracy comparison, and (d) relative accuracy comparison (where the horizontal axis represents the feature number and the vertical axis represents an error, the solid line represents the feature point coordinate error on point clouds and total station measurement data after calibration, and the dotted line represents the error before calibration).

was divided into three processes (see Figure 8). First, the driving trajectory was calculated, and the IMU data and GNSS data were tightly coupled by the Kalman filter algorithm to output the trajectory data. Second, according to the design parameters of the system, spatial registration of trajectory data and original LiDAR data were carried out, the target sphere was fitted from the initial point cloud to calculate the coordinates and parameters of the centre, and then the system mounting parameters were estimated by the calibration model of equation (1). Lastly, spatial registration was performed again using the calibration parameters to get the calibrated point cloud.

4. Results and Discussion

The measurement coordinates of the total station, before and after calibration coordinates of the spherical target centre, and other feature points in the experiment are shown in Table 1. Among them, the first six lines are the spherical centre coordinates of the target ball, which are used to perform system calibration and other data are used to check the calibration accuracy.

The result from the experiment can be discussed by two methods: quantitative evaluation and qualitative evaluation. The quantitative evaluation can reflect the overall accuracy of the VLS system by calculating the relative accuracy and absolute accuracy of the point cloud with the root mean square error (RMSE) formula, and the qualitative evaluation can evaluate the feasibility of calibration by comparing the changes of point clouds before and after calibration. Also, the accuracy is verified by international common third-party software.

4.1. Quantitative Accuracy Evaluation. The absolute accuracy and relative accuracy of the point cloud were calculated by the calibrated feature point coordinates and the measured value of the total station. The coordinates of the spherical centre and other feature points measured by the total station as true values were used to calculate the coordinate error, and then the mean square error was calculated according to the RMSE formula. The absolute accuracy includes the plane accuracy and elevation accuracy of the point cloud, which is calculated by the coordinate values in Table 1, and the error of each point is shown in Table 2, while the relative accuracy is calculated according to the distance between two feature points or the length of a feature in the point cloud, such as the distance between the target balls, building length, road width, and window height, as shown in Table 3. Before the calibration, the error in X and Y, and elevation directions were less than 0.3 m and the relative error was within 0.08 m. After calibration, the error in all three directions and relative error were significantly reduced (see Figure 9). The ability of the calibration method to reduce the misalignment from about 0.3 m to less than 0.1 m and the mean square errors of plane, elevation, and relative accuracy were 0.046 m, 0.078 m, and 0.018 m, respectively. It can be seen that the accuracy of the point cloud after calibration is significantly improved, which meets the accuracy requirements of actual measurement.

4.2. Qualitative Accuracy Evaluation. A qualitative accuracy analysis was performed by comparing the errors between the same point cloud before and after calibration. The comparison results of point clouds in different scenes are shown in Figure 10, where white represents the point cloud after calibration and pink represents the point cloud before

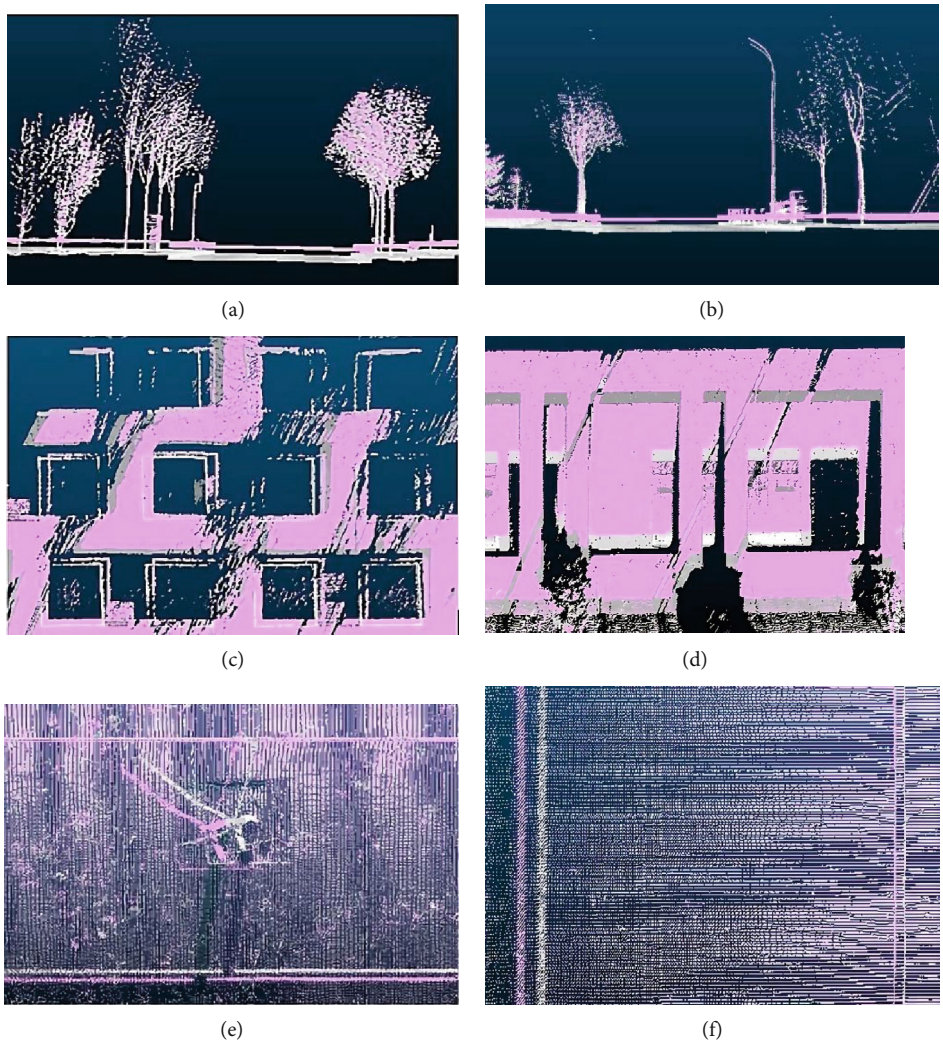

Figure 10: Comparison of the point clouds before and after calibration. (a, b) Elevation deviation, including roads, roadside features, and trees in different directions; (c) building deviation from windows of a certain height; (d) building deviation from the wall near the ground; (e) pavement deviation; and (f) road deviation.

calibration. After calibration, the plane and elevation position of the point cloud changed obviously, which indicates that the point cloud has been significantly improved.

4.3. Accuracy Verification of Third-Party Software. Finally, the point cloud of VLS was registered to the TLS point cloud model for 3D and 2D analysis by using international third-party software. In general, ground point cloud data are more accurate [28] and used as benchmark data for comparison. Since the two scanning ranges did not strictly coincide, the error of the point cloud boundary was large while the error in the area where the point cloud was concentrated and overlapped was small. The 3D analysis calculated all points in the point clouds and represented the analysis results with points of different colours. We selected the point cloud of the building and road for the 3D analysis. The standard deviation was 0.0311 m, and the comparison results in different directions are shown in Figure 11.

A 2D analysis was used to analyze the intercepted point cloud (see Figure 12), reflecting the point cloud accuracy at a certain location. The road point cloud was relatively dense and showed the highest accuracy, and the standard deviation was 0.0083 m. The standard deviation of the building point cloud cross-section was 0.0178 m, and the standard deviation of the longitudinal section was 0.0211 m.

The above accuracy analysis verifies the feasibility of the proposed calibration method based on the target ball. It is worth noting that there must be three common points in the calibration model to calculate the mounting parameters of the system. In the experiment, we set up six target balls for calibration. The number of target balls meets the requirements, and there are redundant observations. The point cloud accuracy after calibration also shows that the number of target balls is reasonable and can be calibrated with sufficient accuracy. To analyze the relationship between the calibration accuracy and the number of target balls, we experimented with the condition of no redundant observation, one redundant observation, and two redundant observations; that is, we selected three, four, and five target balls in the existing experimental conditions. The comparison

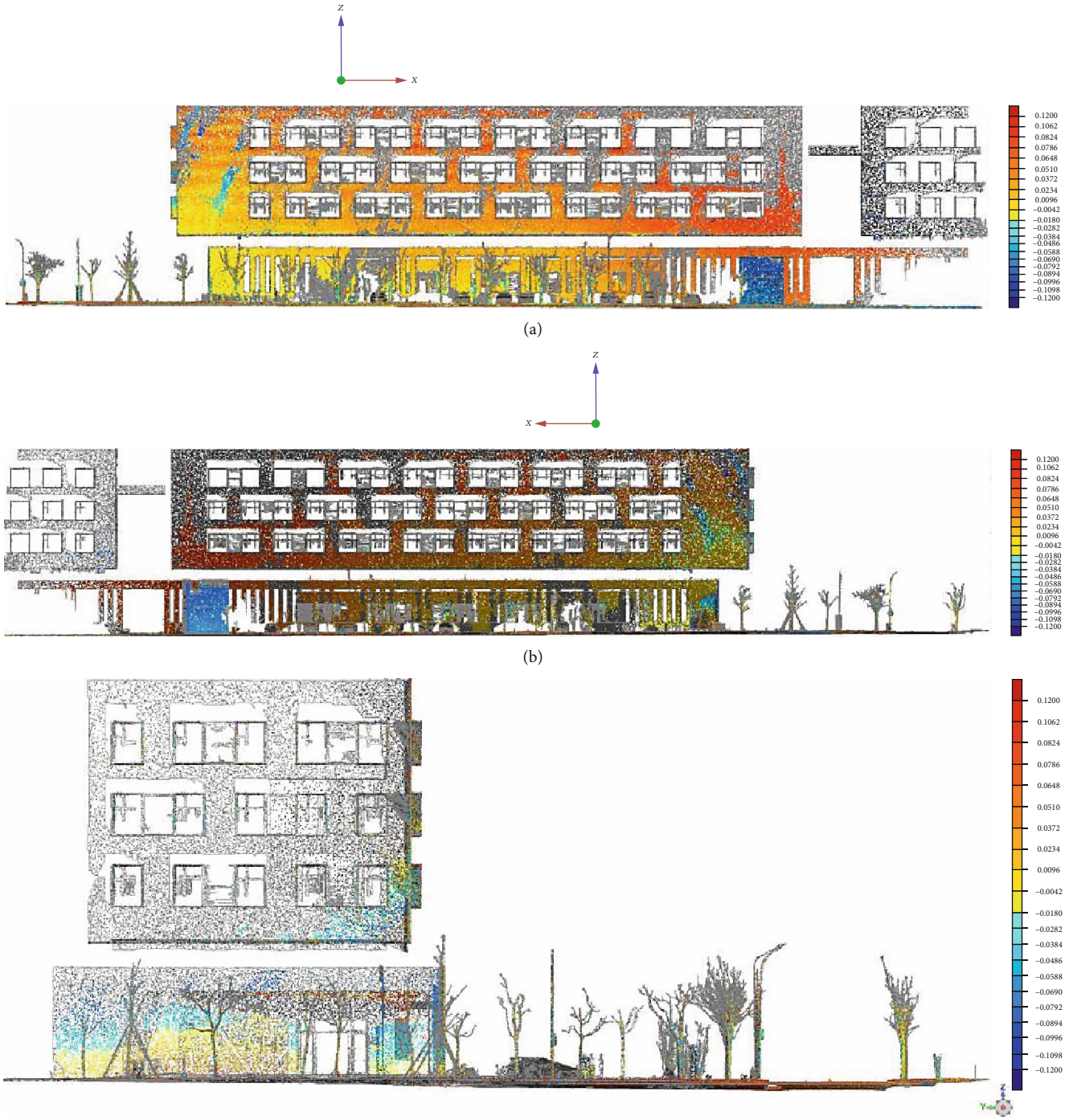

(a)

(b)

(c)

Figure 11: Continued.

(d)

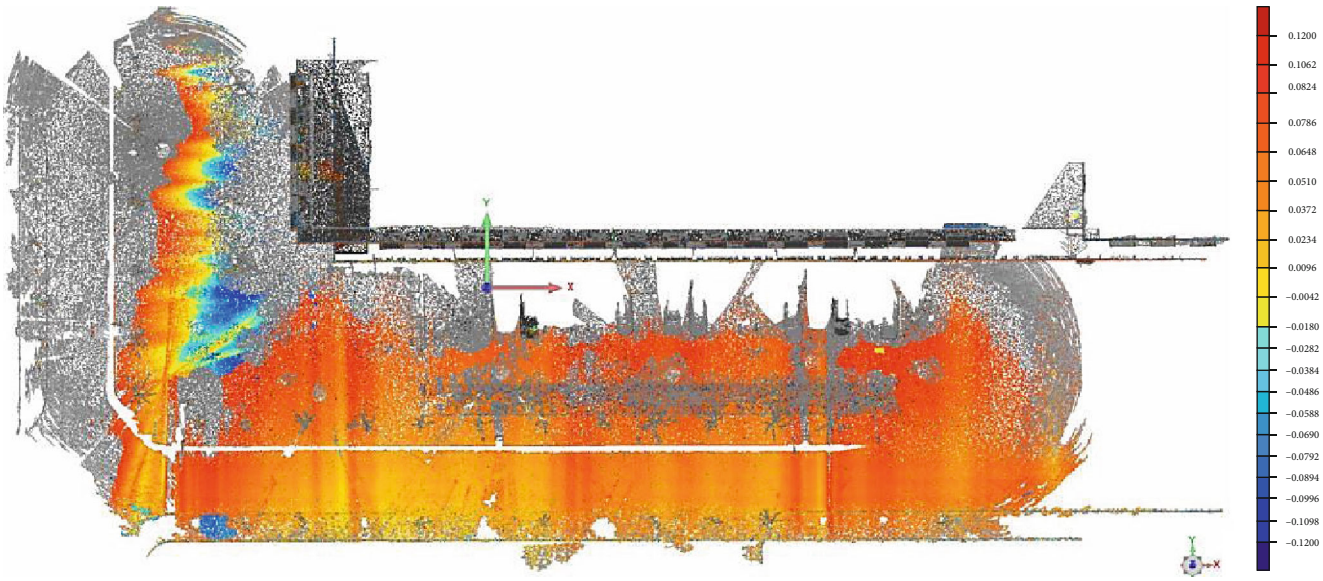

(e)

Figure 11: Continued.

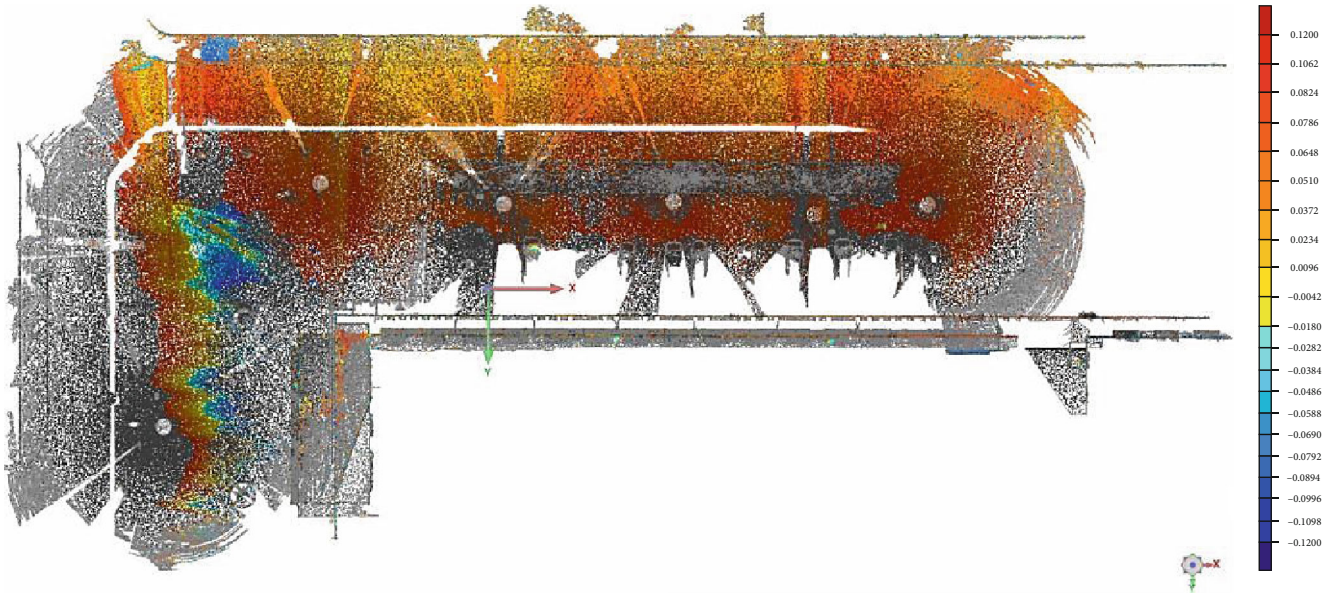

(f)

Figure 11: Results of the 3D analysis. (a) Front view, (b) rear view, (c) left view, (d) right view, (e) top view, and (f) bottom view (points that do not coincide in the edge area are not involved in the calculation, and the colour is displayed in grey. The higher the accuracy, the lighter the colour of the point in the area).

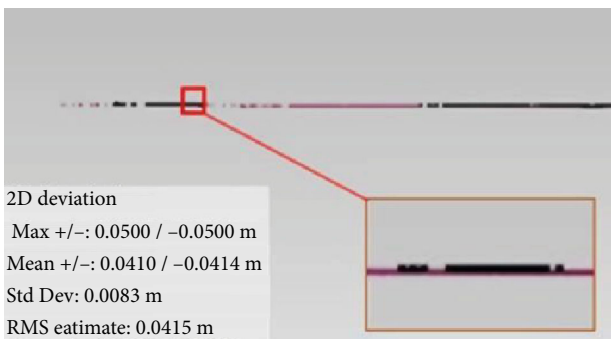

(a)

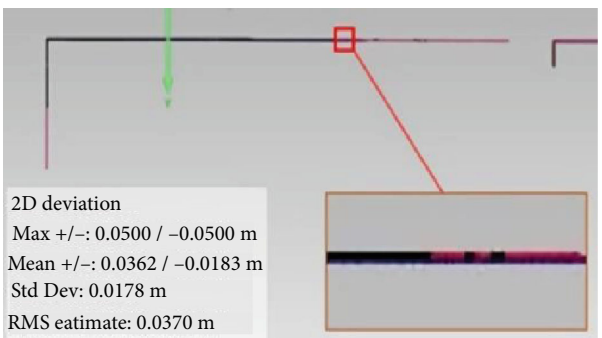

(b)

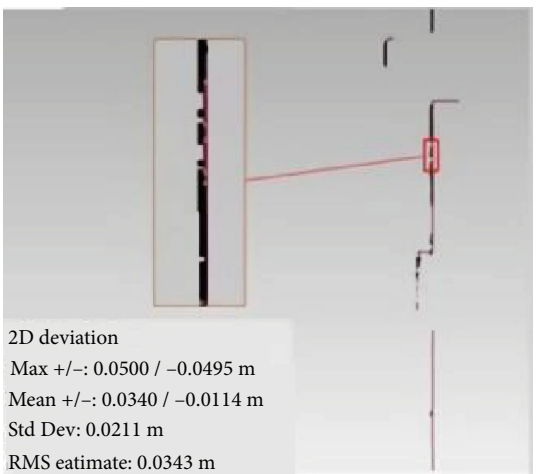

(c)

Figure 12: Results of the 2D analysis. (a) Pavement section, (b) building cross-section, and (c) longitudinal section of a building (the red box is an enlarged display of analysis results, and the lower-left corner is the error analysis results using software).

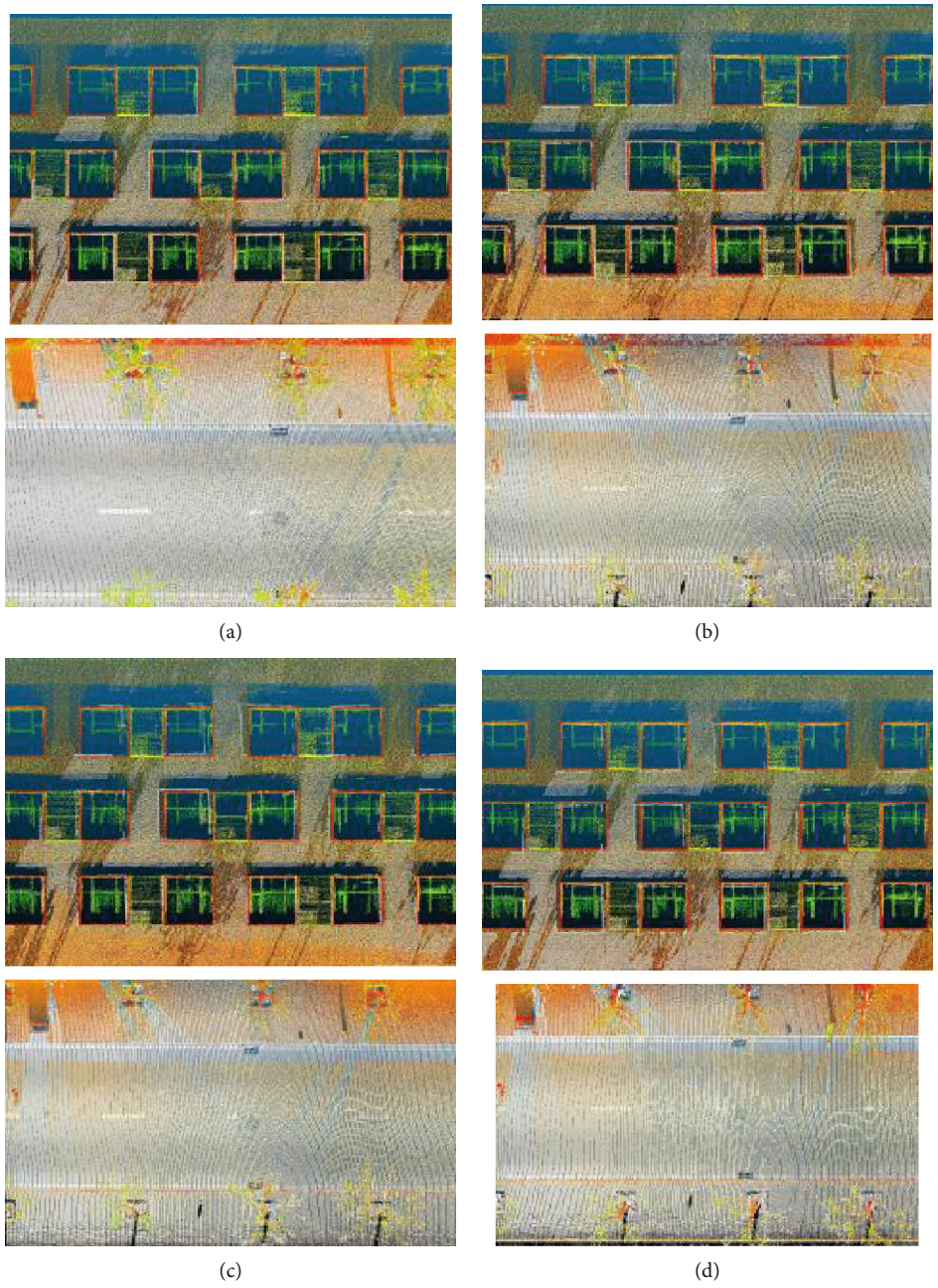

Figure 13: The resulting point cloud of the building facade and road surface after calibration of different numbers of target balls. (a) 6 balls, (b) 5 balls, (c) 4 balls, and (d) 3 balls.

results of the point clouds of the building facade and road surface after calibration are shown in Figure 13 below, in which the pseudocolour represents the point cloud data of TLS and grey represents the point cloud of the VLS system. It can be seen that the accuracy of the point cloud calibrated by the three balls is relatively low, and the accuracy is improved when there are redundant observations, and the point cloud effect of the six balls is relatively the best. In addition, in practical application, considering the problem of experimental cost, through five or six target balls, we can complete the high-precision calibration at low cost. Therefore, using five or six target balls is a better solution, which can not only control the cost but also achieve enough precision calibration.

5. Conclusions

The paper proposes a system calibration method with a self-made special target ball to improve the accuracy of the VLS system. The target ball is designed to alleviate the influence of laser point sparsity on the calibration and ensure that the station instrument measurement is the same location. Taking the centre of the spherical target as a calibration point, the centre coordinates and parameters of the target ball in the

laser point cloud can be accurately calculated by the linear difference; simultaneously, the total station measurement is taken as the true value. According to the calibration model, the mounting parameters of the VLS system are estimated by two least-squares adjustments. We make quantitative and qualitative analyses on the accuracy of the point cloud reconstructed by the calibrated parameters. The plane, elevation, and relative accuracy of the point cloud are 0.046 m, 0.078 m, and 0.018 m, respectively, which achieves better accuracy and is significantly improved compared with the prior calibration. The results indicate that the method effectively improves the accuracy of the VLS point cloud. It provides an effective guarantee for the application of VLS data and contributes to expanding the application field of the VLS system. While the precision achieved by the system is considered sufficient for some applications in this study work, there are a few aspects of the calibration that can be improved. The accuracy of the system is relatively low in areas where the wave fluctuation is serious and the road turns. Future studies will focus on improving the local point clouds, which will improve the overall accuracy and stability of the system. It is a committment to effectively promote VLS systems to play an active role in spatial information collection.

Conflicts of Interest

The authors declare that there are no conflicts of interest regarding the publication of this paper.

Acknowledgments

The authors would like to thank all the institutions that provided funding support for this work. This research was supported by the National Natural Science Foundation of China (grant number 41971350); the Beijing Advanced Innovation Centre for Future Urban Design, Beijing University of Civil Engineering and Architecture (grant number UDC2019031724); and the Beijing University of Civil Engineering and Architecture Pyramid Talent Training Project Lecturer Teacher Support Plan (JDJQ20200307).

References

[1] M. Guo, G. L. Wang, C. Chen et al., *Design Principle and Implementation Method of Mobile Mapping System*, Science Press, Beijing, China, 2018.

[2] M. Guo, S. Z. Dong, X. W. Shen, C. Chen, and D. Pan, "Research on calibration technology of vehicle laser scanning system," in *2017 3rd IEEE International Conference on Computer and Communications (ICCC)*, pp. 2889–2893, Chengdu, 2017.

[3] I. Puente, H. Gonzalez, P. Arias, and J. Armesto, "Land-based mobile laser scanning systems: a review," in *ISPRS Int. Arch. of the Photogramm., Remote Sensing and Spatial Information Sciences*, vol. XXXVIII-5/W12, pp. 163–168, ISPRS Calgary 2011 Workshop, Calgary, Canada, 2017.

[4] H. Wang, X. Lou, Y. Cai, Y. Li, and L. Chen, "Real-time vehicle detection algorithm based on vision and LiDAR point cloud fusion," *Journal of Sensors*, vol. 2019, Article ID 8473980, 9 pages, 2019.

[5] N. Sairam, S. Nagarajan, and S. Ornitz, "Development of mobile mapping system for 3D road asset inventory," *Sensors*, vol. 16, no. 3, p. 367, 2016.

[6] X. W. Shen, M. Guo, and S. Z. Dong, "Research on calibration method of vehicle mapping system based on special target," in *International Conference on Computer Science and Application Engineering (CSAE)*, Shanghai, China, 2017.

[7] R. Ravi and A. Habib, "Fully automated profile-based calibration strategy for airborne and terrestrial mobile LiDAR systems with spinning multi-beam laser units," *Remote Sensing*, vol. 12, no. 3, p. 401, 2020.

[8] Y. Q. Ma, X. C. Xu, and Z. Z. Zheng, "Analysis of Trimble MX7 mobile measurement system accuracy influencing factors," *Geomatics& Spatial Information Technology*, vol. 42, no. 4, pp. 62–65, 2019.

[9] W. F. Zhang, J. F. Li, and Y. Chen, "Comprehensive research on accuracy of mobile laser scanning system," *Urban Geotechnical Investigation & Surveying*, vol. 2018, no. 5, pp. 83–85+89, 2018.

[10] M. Yadav, S. Goel, A. K. Singh, and B. Lohani, "Developing basic design and mathematical framework for a mobile mapping system—a case study using available sensors," *Journal of the Indian Society of Remote Sensing*, vol. 42, no. 2, pp. 301–310, 2014.

[11] I. Detchev, A. Habib, M. Mazaheri, and D. Lichti, "Practical in situ implementation of a multicamera multisystem calibration," *Journal of Sensors*, vol. 2018, Article ID 5351863, 12 pages, 2018.

[12] Y. Song, Z. G. Gao, and C. H. Li, "Discussion on accuracy test of mobile laser measurement system," *Science of Surveying and Mapping*, vol. 40, no. 9, pp. 74–77+97, 2015.

[13] C. Glennie, "Calibration and kinematic analysis of the Velodyne HDL-64E S2 LiDAR sensor," *Photogrammetric Engineering and Remote Sensing*, vol. 78, no. 4, pp. 339–347, 2012.

[14] J. Y. Han, C. S. Chen, and C. T. Lo, "Time-variant registration of point clouds acquired by a mobile mapping system," *IEEE Geoscience and Remote Sensing Letters*, vol. 11, no. 1, pp. 196–199, 2014.

[15] M. He, H. Zhao, F. Davoine, J. Cui, and H. Zha, "Pairwise LIDAR calibration using multi-type 3D geometric features in natural scene," in *2013 IEEE/RSJ International Conference on Intelligent Robots and Systems*, pp. 1828–1835, Tokyo, Japan, 2013.

[16] X. G. Tian, X. L. Jun, T. Xu, X. L. Li, and Q. T. Zhang, "Calibration of angles for mobile LiDAR scanner system," *Infrared and Laser Engineering*, vol. 43, no. 10, pp. 3292–3297, 2014.

[17] S. Hong, L. Park, J. Lee, K. Lim, Y. Choi, and H. G. Sohn, "Utilization of a terrestrial laser scanner for the calibration of mobile mapping systems," *Sensors*, vol. 17, no. 3, 2017.

[18] K. Julge, T. Vajakas, and A. Ellmann, "Performance analysis of a compact and low-cost mapping-grade mobile laser scanning system," *Journal of Applied Remote Sensing*, vol. 11, no. 4, 2017.

[19] T. O. Chan, D. D. Lichti, and C. L. Glennie, "Multi-feature based boresight self-calibration of a terrestrial mobile mapping system," *ISPRS journal of photogrammetry and remote sensing*, vol. 82, no. 82, pp. 112–124, 2013.

[20] W. T. Zhang, W. H. Zhang, and L. Z. Wang, "Research and application of utilizing UAV laser radar to perfect

the vehicle-borne mobile mapping systems data," *Bulletin of Surveying and Mapping*, vol. 2018, no. 10, pp. 98–101, 2018.

[21] Z. Li, J. Tan, and H. Liu, "Rigorous boresight self-calibration of mobile and UAV LiDAR scanning systems by strip adjustment," *Remote Sensing*, vol. 11, no. 442, 2019.

[22] F. Wang, Y. Zhuang, H. Gu, and H. Hu, "Automatic generation of synthetic LiDAR point clouds for 3-D data analysis," *IEEE Transactions on Instrumentation and Measurement*, vol. 68, no. 7, pp. 2671–2673, 2019.

[23] M. Guo, Y. M. Wang, G. L. Wang, and Z. L. Wang, "A multifunctional and practical LiDAR scanning target," China Patent ZL201410422162.4, 2017.

[24] S. Haughey, C. Deegan, M. Brogan, C. Fitzgerald, S. McLoughlin, and S. Murray, "Mobile mapping system for the automated detection and analysis of road delineation," *IET Intelligent Transport Systems*, vol. 5, no. 4, pp. 221–230, 2011.

[25] Q. LIU, *Calibration Method of Mobile Photogrammetric Mapping System*, PLA Information Engineering University, 2013.

[26] S. Madeira, J. A. Gonçalves, and L. Bastos, "Sensor integration in a low cost land mobile mapping system," *Sensors*, vol. 2012, no. 12, pp. 2935–2953, 2012.

[27] A. Abd-Elrahman, N. Sassi, B. Wilkinson, and B. Dewitt, "Georeferencing of mobile ground-based hyperspectral digital single-lens reflex imagery," *Journal of Applied Remote Sensing*, vol. 10, article 014002, no. 1, 2016.

[28] H. B. Wu, M. Scaioni, H. Y. Li, N. Li, M. Lu, and C. Liu, "Feature-constrained registration of building point clouds acquired by terrestrial and airborne laser scanners," *Journal of Applied Remote Sensing*, vol. 8, no. 1, article 083587, 2014.